Thai Journal of **Math**ematics
Volume 19 Number 3 (2021)
Pages 1082–1095

http://thaijmath.in.cmu.ac.th

ISSN 1686-0209

Application of Finite Volume Method with Unstructured Quadrilateral Mesh for Solving 2-D Magnetotelluric Modeling

Tanapon Khampichit and Weerachai Sarakorn*

Department of Mathematics, Faculty of Science, Khon Kaen University, Khon Kaen, 40002, Thailand.
Smart Learning Innovation Research Center, Khon Kaen University, Khon Kaen, 40002, Thailand.
e-mail : k.tanapon27@gmail.com (T. Khampichit); wsarakorn@kku.ac.th (W. Sarakorn)

Abstract This paper presents 2-D magnetotelluric (MT) modeling with finite volume (FV) method incorporating unstructured quadrilateral mesh. The accuracy, efficiency, and reliability are presented and compared to other numerical methods. The numerical results indicate that our FV method provides good accuracy when the appropriate mesh is incorporated. The reliability of the developed FV scheme is also confirmed with both analytical values and COMMEMI projects. In addition, our developed FV codes with unstructured quadrilateral mesh show valuable and powerful features such as handling the irregular and complex subregions.

MSC: 86-08; 65M08; 65M50
Keywords: 2-D magnetotelluric modeling; finite volume method; unstructured quadrilateral mesh

Submission date: 26.04.2021 / Acceptance date: 23.07.2021

1. Introduction

Several numerical techniques such as finite difference (FD) method [14, 18], finite element (FE) method [5, 9, 10, 15, 17, 18, 22, 23], and finite volume (FV) method [4] are developed and implemented for 2-D magnetotelluric (MT) forward modeling. The FD method is the numerical technique that is often used for some simple models. However, the FD method cannot handle some real-world models, including many complex subregions such as terrain, seafloor, and irregular anomalous substructures, because it has a limitation on the rectangular mesh. With these problems, the FE and FV methods are proven to overcome those problems because both methods can incorporate several unstructured mesh types for handling complex substructures. Presently, the accuracy and efficiency of the FE method for 2-D MT modeling have been proven [5, 9, 10, 15, 17, 22, 23]. For the FV method, it is now gained and has more attention. Evidence of its efficiency

*Corresponding author.

Published by The Mathematical Association of Thailand.

and accuracy can be found in MT modeling [4, 6] and 2-D reservoir simulation problem [7]. The FV scheme with structured mesh and unstructured tetrahedral mesh have successfully applied to both 2-D and 3-D MT modeling [4, 6]. In the present, some advantages of unstructured quadrilateral mesh with FE method and FV method can be found in [7, 17]. In the present, there is no application of the FV scheme with unstructured quadrilateral mesh for MT modeling. So, it is exciting and challenging to use the unstructured quadrilateral mesh for the FV method to solve 2-D MT modeling.

In this work, the alternative FV method incorporating with unstructured quadrilateral mesh for solving 2-D MT modeling is proposed. The FV codes employing the paving algorithm [1] to generate the unstructured quadrilateral mesh were developed on MATLAB programming. The accuracy, efficiency, and reliability of our FV method will be presented and tested on various 2-D benchmark models.

2. 2-D Magnetotellurics modeling

MT modeling describes the behavior of the natural electromagnetic (EM) interacting with the Earth. The naturally occurring EM fields are considered as a harmonic plane-wave with neglecting displacement currents. Here, the time dependence is assumed to be $e^{-i\omega t}$, where ω is the angular frequency. For the 2-D case, we assume that the strike direction (the direction that the resistivity's structure does not change) is paralleled to the $x-$direction. Therefore, the resistivity $\rho = \rho(y, z)$. The governing equations for the 2-D MT problem with the bounded domain $\Omega \subset \mathbb{R}^2$ are given by

$$\nabla \cdot \alpha \nabla U + \beta U = 0. \tag{2.1}$$

The notations α, β and U denote different representations depending on the two MT modes:

The Transverse Electric (TE) mode: $U = E_x, \alpha = 1, \beta = i\omega\mu/\rho$,

The Transverse Magnetic (TM) mode: $U = H_x, \alpha = \rho, \beta = i\omega\mu$,

where E_x and H_x are the electric and magnetic fields, respectively, μ is the magnetic permeability in free space. Here, $\mu = \mu_0 = 4\pi \times 10^{-7}$ Vs/Am. For the 2-D problem, the computing domain is defined as a region $\Omega \subset \mathbb{R}^2$.

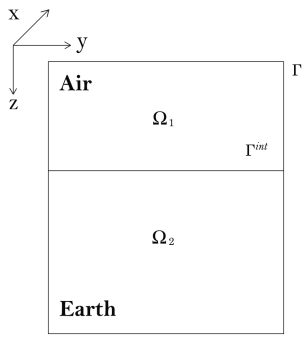

Figure 1. Graphical representation of computing domain for the 2-D problem.

As illustrated in Figure 1, $\Omega = \Omega_1 \cup \Omega_2 \cup \Gamma \cup \Gamma^{int}$, where the subregion Ω_1 is defined as the air layer, the subregion Ω_2 is defined as the earth layer, the boundary Γ is the outer boundary, and Γ^{int} is the air-earth interface. The partial differential equation (2.1) subjected to the Dirichlet boundary conditions:

$$U = U_0(y, z) \in \Gamma, \tag{2.2}$$

where $U_0(y,z)$ is obtained by solving the 1-D problem analytically or numerically [5].

3. Unstructured Quadrilateral Mesh

To incorporate the unstructured quadrilateral mesh for the FV method. Here, the mesh algorithm called the paving algorithm[1] is implemented. The concept of the paving algorithm for the 2-D model have been illustrated in [17]. Its idea is summarized again in Figure 2.

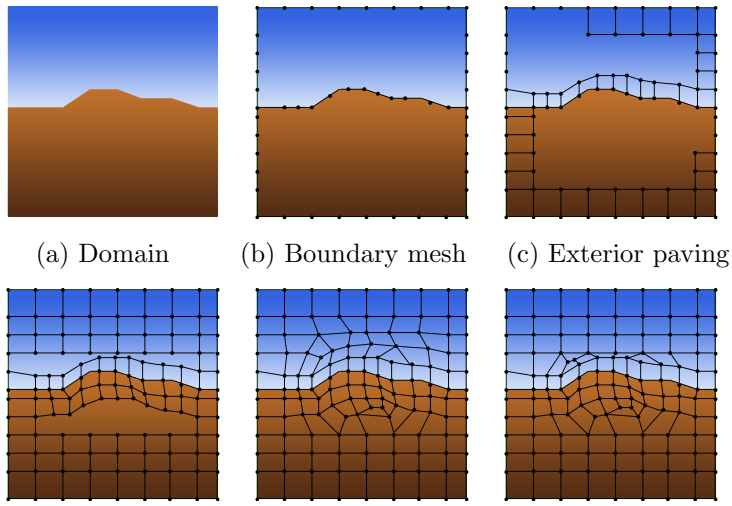

(a) Domain (b) Boundary mesh (c) Exterior paving

(d) Row generation (e) Seam (f) Cleanup

Figure 2. The paving algorithm for 2-D model[17].

It is started with meshing on a boundary (Fig. 2 b) and is followed by the interior paving. The boundary is paved clockwise and progresses outward from the permanent interior boundary. This step is called row choice (Fig. 2 c). Then, adding and adjusting new rows to edit the element size and improve the mesh quality using the smoothing process and row adjustment, respectively, are applied (Fig. 2 d). When rows is begun to overlap at the inside of the subregions, the validity of mesh is checked by using the seaming process (Fig. 2 e). Finally, the cleanup process, the process that re-adjusted to improve the aspect ratio in the local, reduce the number of irregular nodes, or eliminate elements with bad internal angles by removing and/or adding an volume, is taken to obtain the completed unstructured quadrilateral mesh (Fig. 2 f).

In this paper, Trelis commercial software is taken to create the unstructured quadrilateral mesh for FV method. All information of quadrilateral volumes, including the nodal

coordinates and nodal volumes (node indices surrounding each volume) are required for our FV MATLAB codes.

4. Finite volume method

To apply the FV method to the governing equations (2.1), the element-based finite volume (EbFV) method is chosen. With the EbFV concept, the conservation of mass is enforced over polygonal control volume (CV) constructing in a vertex-centered FV method. This yields the discrete equation is physically balance over CVs [7]. As shown in Figure 3, the considered domain is now composed of quadrilateral elements or volumes by using unstructured quadrilateral mesh. Each CV is set up by neighborhoods volumes.

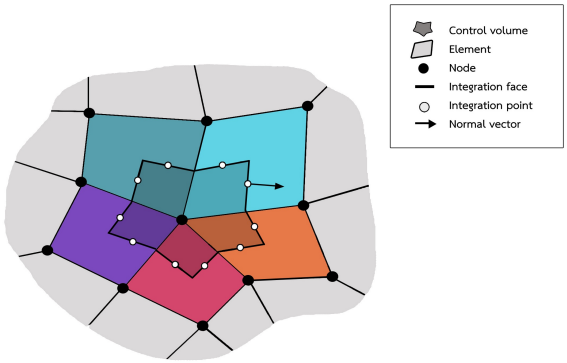

Figure 3. Constructing the CV based on the EbFV method.

Each unknown is set and calculated at each node located at every volume corner. The equation of each CV is constructed by forming the portions of the volumes that share a common node. A certain face area delimits every CV. For each CV, we assume that the residual of the (2.1) is $r = \nabla \cdot \alpha \nabla U + \beta U$. Here, U is assumed to be an approximated solution by the FV method. The EbFV method try to seek a minimization of the non-weighted residual by taking double integral over each CV ΔV. Therefore,

$$\iint_{\Delta V} r ds = \iint_{\Delta V} (\nabla \cdot \alpha \nabla U + \beta U) ds. \tag{4.1}$$

Reducing the second-order term by using divergence theorem, the equation (4.1) is expressed as

$$\iint_{\Delta V} r ds = \int_{\cup \Delta S_i} (\alpha \nabla U) \cdot dS + \iint_{\Delta V} \beta U dV, \tag{4.2}$$

where $\cup \Delta S_i$ is the boundary of CV. The conservation of physical quantities over every CV is the essential premise of the EbFV method. Since the shape of CVs constructed following the described procedure may be extremely complex, a special strategy is required for dealing with the increased geometrical complexity. The strategy employed in the EbFV method taken from the FE technique defines the local coordinate system ξ, η instead of the

real $yz-$coordinate inside every element by the coordinate transformation. The graphical representation of transformation is illustrated in Figure 4.

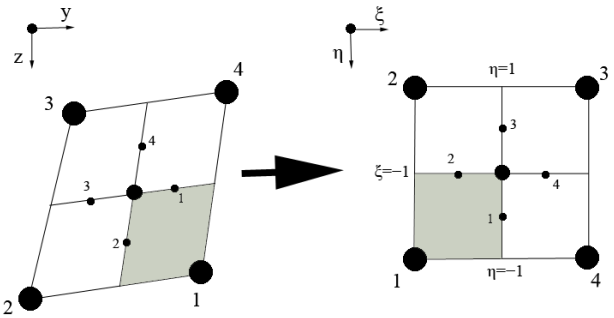

FIGURE 4. Coordinate transformation between quadrilateral volume in real coordinate and 2-unit square volume in local coordinate.

Therefore, all calculations can be easily made based upon the geometry of a standard transformed element. Then, the conservation equations of every CV can be assembled using the contributions coming from all neighboring volumes. For quadrilateral shape, the coordinate transformation can be conveniently expressed employing the following bilinear shape functions [8]

$$U_x^e(y,z) = \sum_{j=1}^{N^e} S_j^e(\xi,\eta) u_j^e, \tag{4.3}$$

where S_j^e are the real-valued basis functions, u_j^e are the unknown coefficients with complex-valued, and N is the number of nodes per element. In this case, $N^e = 4$ for the linear quadrilateral shape. For simplicity, the basis functions are defined in new coordinates and are given by

$$\left.\begin{aligned} S_1^e(\xi,\eta) &= \frac{1}{4}(1-\xi)(1-\eta) \\ S_2^e(\xi,\eta) &= \frac{1}{4}(1+\xi)(1-\eta) \\ S_3^e(\xi,\eta) &= \frac{1}{4}(1+\xi)(1+\eta) \\ S_4^e(\xi,\eta) &= \frac{1}{4}(1-\xi)(1+\eta) \end{aligned}\right\}, \tag{4.4}$$

where (ξ,η) is the local coordinates. The expressions of the transformation are given by

$$\left.\begin{aligned} y(\xi,\eta) &= \sum_{j=1}^{4} s_j^e(\xi,\eta) y_j^e \\ z(\xi,\eta) &= \sum_{j=1}^{4} S_j^e(\xi,\eta) z_j^e \end{aligned}\right\}, \tag{4.5}$$

where (y, z) are the real coordinates of the $j-$th node. Next, consider the line integral in the first term of (4.2). The line integrals is approximated by using the midpoint rule [7], we obtain

$$\int_{\cup \Delta S_i} (\alpha \nabla U) \cdot dS = \sum_e [\sum_i (\alpha \nabla U)_i \cdot \Delta S_i]_e, \tag{4.6}$$

where i denotes the integration points locating at face centers. ΔS_i denotes the face area vector that point outside of the CV. Using bilinear approximation, the inner term in (4.6) can be expressed as

$$[\alpha_i (\nabla U)_i \cdot \Delta S_i]_e \approx (\alpha_i)[D]_i^T [u]_e, \tag{4.7}$$

where u_e is a column vector whose components are located at the four node of the element e and $[D]_i^T$ is a row vector defined by

$$[D_{\xi,\eta}]_i^T = [S]_i ([W]_i^T [J]_i^{-1})[\bar{n}^*]_i, \tag{4.8}$$

where $[S]_i$ is the basis function, $[W]_i$ and $[J]_i$ are the derivatives matrix that calculated at the integration point i and $[\bar{n}^*]_i$ is the coordinates of the normal vectors. Next, assembling the discrete equation (4.6) for each CVs yields

$$\sum_e [\sum_i (\alpha \Delta U) \cdot \bar{n}]_e \approx \begin{bmatrix} \alpha_1[\beta]_1^T - \alpha_1[\beta]_4^T \\ \alpha_1[\beta]_2^T - \alpha_1[\beta]_1^T \\ \alpha_1[\beta]_3^T - \alpha_1[\beta]_2^T \\ \alpha_1[\beta]_4^T - \alpha_1[\beta]_3^T \end{bmatrix} \begin{bmatrix} u_1 \\ u_2 \\ u_3 \\ u_4 \end{bmatrix} = [A]_e [u]_e, \tag{4.9}$$

the matrix $[A]_e$ is an volume matrix for volume (e). Each row of this matrix is related to one of the four adjoining CVs and includes two contributions.

For the second term in (4.2), the double integral over volume can be evaluated numerically using Gauss-Quadrature rule for each quadrilateral volume. This yields

$$\iint_{\Delta V} \beta U dV = [K]_e [u]_e. \tag{4.10}$$

Substituting (4.9) and (4.10) into (4.2) and rearranging terms, we get

$$\iint_{\Delta V} r ds = ([A]_e + [K]_e)\,[u]_e. \tag{4.11}$$

Assembling (4.11) for all quadrilateral volumes in the given mesh and enforcing to zero, i.e.

$$\iint_{\Omega} r ds = \sum_{e=1}^{M} \iint_{\Delta V} r ds = \sum_{e=1}^{M} (([A]_e + [K]_e)\,[u]_e) = 0, \tag{4.12}$$

where M is the total number of volumes. Finally, the obtained system of equation is expressed as

$$[K][u] = [b], \tag{4.13}$$

where $[K]$ is the coefficient matrix, $[u]$ is the unknown vector, and $[b]$ is the source vector corresponding to the Dirichlet boundary conditions. The system of the equations in (4.13) is solved by LU factorization. Once the electric and magnetic fields are obtained, taking the ratio between the orthogonal electric and the magnetic fields yields the impedances.

The impedances for TE-and TM modes, denoted by Z_{xy} and Z_{yx}, respectively, are defined by

$$Z_{xy} = \frac{E_x}{H_y}, Z_{yx} = \frac{H_x}{E_y}. \tag{4.14}$$

Finally, the apparent resistivity, denoted as ρ and phase, denoted as ϕ , can be evaluated by

$$\rho_{ij} = \frac{1}{\omega\mu}|Z_{ij}|^2, \tag{4.15}$$

and

$$\phi_{ij} = \arg(Z_{ij}), \tag{4.16}$$

where $i,j = y,z$. Note that, the responses Z_{ij}, ρ_{ij}, and ϕ_{ij} are calculated at desired sites on the earth's surface or seafloor.

5. Numerical Results

In this section, the accuracy and efficiency of our FV codes are presented, compared, and discussed. The models designed and selected for this section are half-space, three-layered, and COMMEMI2D-4 models [23]. Our FV codes are developed under MATLAB programming and modified from the FE codes developing by [17]. The commercial software is used to generated the unstructured quadrilateral mesh. Then, the information of nodes and volume inside the domain is imported as input files for our FV codes. All numerical tests are computed and run on a computer desktop with CPU 1.99 GHz and RAM 4 GB.

5.1. Half-space model

The simple half-space model used to test accuracy is illustrated in Figure 5 (left). The size of this model is designed as 400 km × 200 km. Here, the thickness of the air layer is extended to 200 km. The earth's surface is assumed to be flat and homogeneous clay with resistivity of 100 ohm-m. Here, we assume that there are 19 sites in the range −30 km to 30 km with a distance 3 km located on the earth's surface ($z = 0$ km) . The apparent resistivity and phases are computed at 4 periods: T $= 0.1, 1.0, 10,$ and 100 s for both TE and TM modes. The resistivity model of this model is shown in Figure 5 (left).

To solve 2-D MT modeling by using FV method, the given model is discretized into unstructured quadrilateral mesh with many volumes and nodes. The computing domain and its generated mesh are shown in Figure 5 (right). The smallest volume's size (minimum edge's length of volume) around MT sites is set as 100 m. The size of the volumes which located far away from the sites and the interested area are increased with rate 1.2 and 1.4 for both earth and air layers. The total number of generated nodes and volumes are $20,725$ and $20,696$, respectively. Note that, the given mesh information is identical to those of [17] used for the FE method.

For each period, our FV algorithm takes about 250 seconds to finish the task. For this model, the exact apparent resistivity at each site is identical to the assumed resistivity, i.e., 100 ohm-m and the phase is equal to 45 degrees. The root mean square (RMS) errors of the apparent resistivity and phase are shown in Table 1.

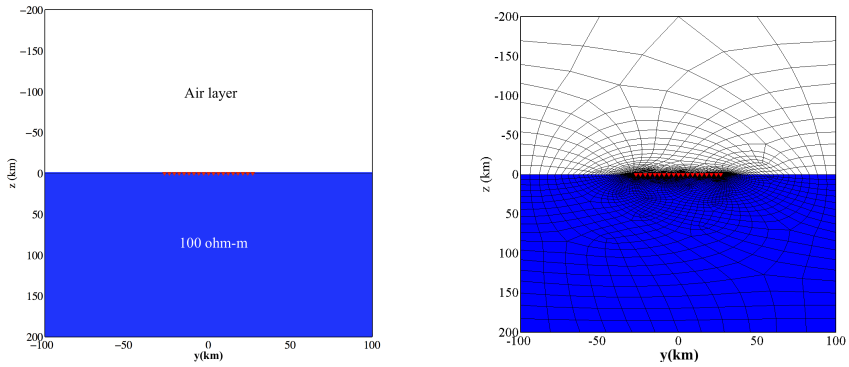

FIGURE 5. The 100 ohm-m homogeneous earth (left) and meshing with unstructured quadrilateral mesh (right). The 19 sites are marked as red triangles [17].

TABLE 1. RMS errors of apparent resistivity and phase of half-space model.

Period(s)	TE-mode		TM-mode	
	ρ_{xy}	ϕ_{xy}	ρ_{yx}	ϕ_{yx}
0.1	0.3265	0.0073	0.5689	0.0460
1	0.2848	0.0111	0.3273	0.0375
10	0.3174	0.0207	0.2807	0.0108
100	0.2969	0.1557	0.0594	0.1482

The maximum RMS errors of apparent resistivity and phase occurred at the shortest tested period at T = 0.1 s, whereas the minimums have occurred at the longest period T = 100 s. The trend of RMS is reduced when the period is increased. The results indicate that our FV codes give good accuracy.

5.2. THREE-LAYERED MODEL

For the second model, the domain is set as 400 km × 200 km. As same as the first model, the thickness of the air layer is extended to 200 km. The 100 ohm-m layer is designed at the top and the thickness of the layer in the left is less narrow than that of the right-hand. The resistivity of the second layer is assigned as 1000 ohm-m. The thickness of the left-hand side is wider than that of the right-hand side. For the rest region at the bottom, the resistivity is 10 ohm-m. The total number of sites is 19 sites with a distance 3 km. The periods of EM wave used to test here are $1, 10, 100$, and 1000 s. The resistivity model is shown in Figure 6 (a).

Since this model is not homogeneous and not horizontal layered model. Then, the analytical apparent resistivity and phases cannot be computed analytically. Thus, the purpose of testing this model is focused on comparison of the solutions obtaining by the fine and coarse mesh instead. For the coarse mesh, the $3,950$ nodes and $3,905$ volumes are generated whereas the $15,709$ nodes and $15,620$ volumes are generated for the fine mesh. Note that the initial mesh size and the grow rate for these two cases are different. The coarse mesh and fine mesh are shown in Figure 6 (b) and 6 (c), respectively.

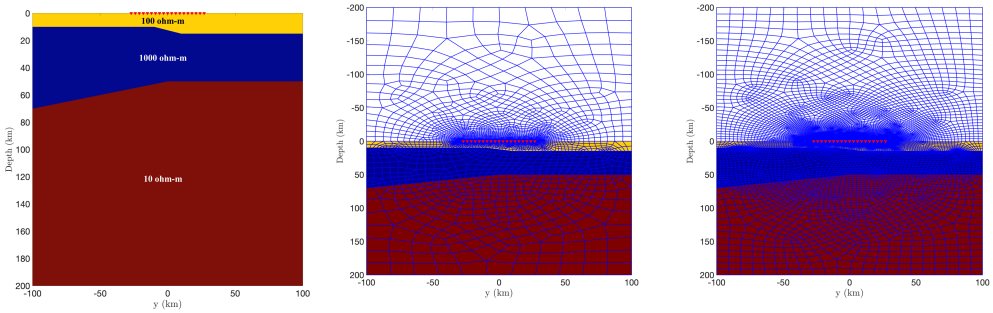

(a) (b) (c)

FIGURE 6. The resistivity model of three-layered model (a). The model with coarse mesh case (b) whereas that with fine mesh case (c). The 19 sites are marked as red triangles.

The apparent resistivity and phases computed at T = 1 s are shown in Figure 7. The maximum difference between the coarse and fine mesh for apparent resistivity and phases are 0.8250 % and 0.3136 %.

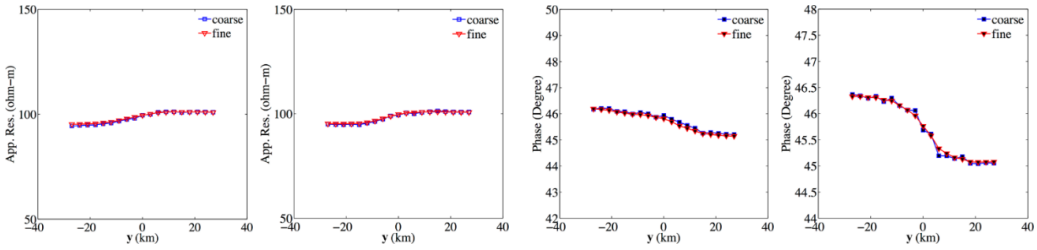

Apparent resistivity for TE-mode (left) and TM-mode(right).

Phase for TE-mode (left) and TM-mode (right).

FIGURE 7. The apparent resistivity and phases: T = 1 second.

At T = 10 seconds, the apparent resistivity and phases are shown in Figure 8. The maximum difference between the coarse and fine mesh for apparent resistivity and phase are 2.3393 % and 0.8076 %, respectively.

At T = 100 seconds, the apparent resistivity and phases are shown in Figure 9. The maximum difference between the coarse and fine mesh for apparent resistivity and phase are 0.7663 % and 0.5393 %, respectively.

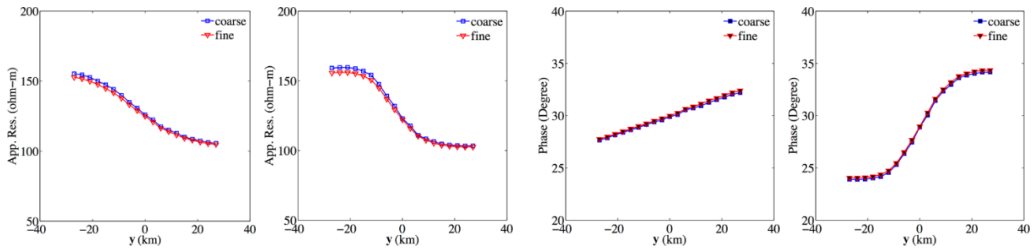

Apparent resistivity for TE-mode (left) and TM-mode(right). Phase for TE-mode (left) and TM-mode (right).

FIGURE 8. The apparent resistivity and phases at period T = 10 seconds.

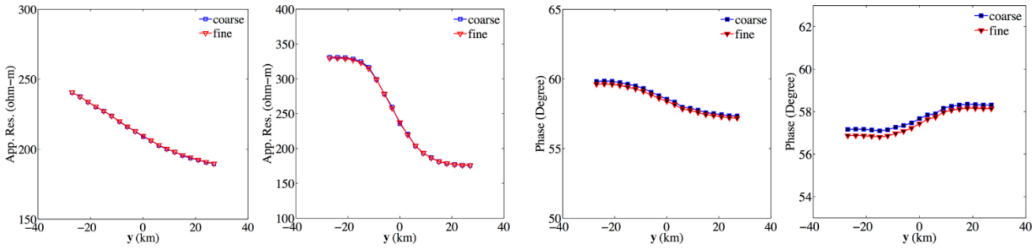

Apparent resistivity for TE-mode (left) and TM-mode(right). Phase for TE-mode (left) and TM-mode (right).

FIGURE 9. The apparent resistivity and phases: T = 100 seconds.

At T = 1000 seconds, the apparent resistivity and phases are shown in Figure 10. The maximum difference between the coarse and fine mesh for apparent resistivity and phase are 1.2503 % and 0.0567 %, respectively.

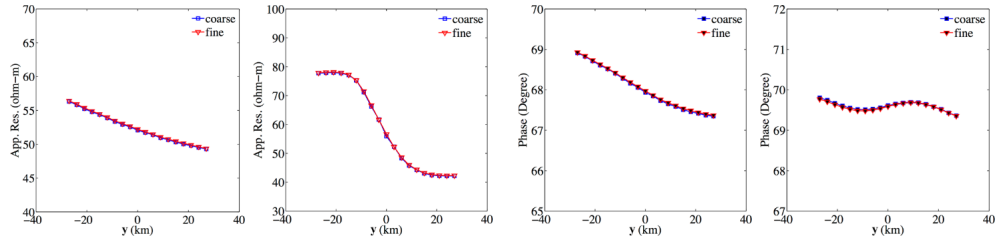

Apparent resistivity for TE-mode (left) and TM-mode(right). Phase for TE-mode (left) and TM-mode (right).

FIGURE 10. The apparent resistivity and phases: T = 1000 seconds.

According to the above results, the FV codes with coarse and fine mesh are comparable. With the appropriate local mesh refinement of unstructured quadrilateral mesh, our FV codes may not need to use very fine mesh for providing the accurated solutions.

5.3. COMMEMI2D-4 MODEL

For the last model, the COMMEMI2D-4 model was proposed by Zhdanov et al.[23] for comparison of modeling methods for electromagnetic modeling. The resistivity model is illustrated in Figure 11 (left). Here, the size of domain is 200 km × 200 km. To solve 2-D MT modeling using FV method, the model is meshed into 18,990 nodes and 18,910 volumes. The smallest element's size is set as 80 m. The close-up of some mesh near earth's surface and shallow depth with local mesh refinement are shown in Figure 11 (right).

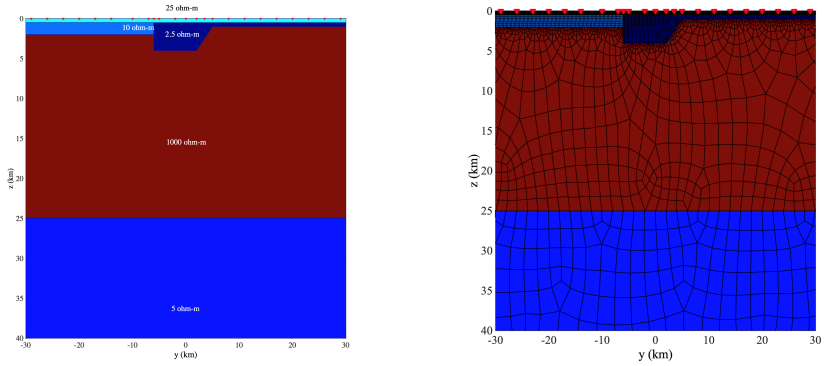

FIGURE 11. The resistivity structure of COMMEMI2D-4 model (right). The 23 sites are marked as red triangles.

The apparent resistivity of 23 sites, where located in range −30 km to 30 km are computed at periods T = 1 and 100 s. At period T = 1 s, the obtained apparent resistivity is shown in Figure 12 and those at T = 100 s are shown in Figure 13.

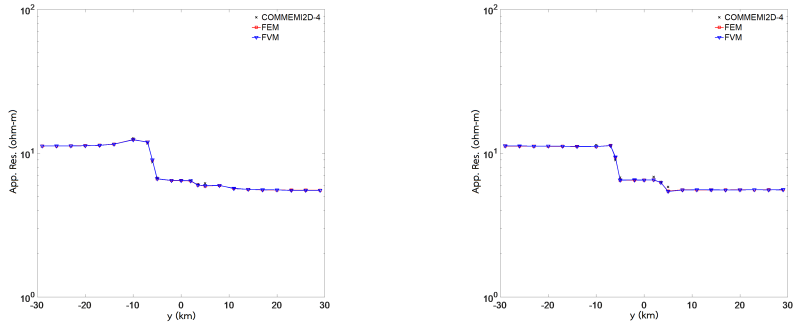

FIGURE 12. Apparent resistivity at period T = 1 second for TE-mode (left) and TM-mode (right).

Our numerical results quite agree and comparable with those of COMMEMI2D-4 projects and FE codes [17]. The errors of apparent resistivity for TE-mode are less than those of TM-mode. These comparisons confirm the validity and reliability of our FV codes. Since the processing to construct the coefficient matrix obtaining by the FV

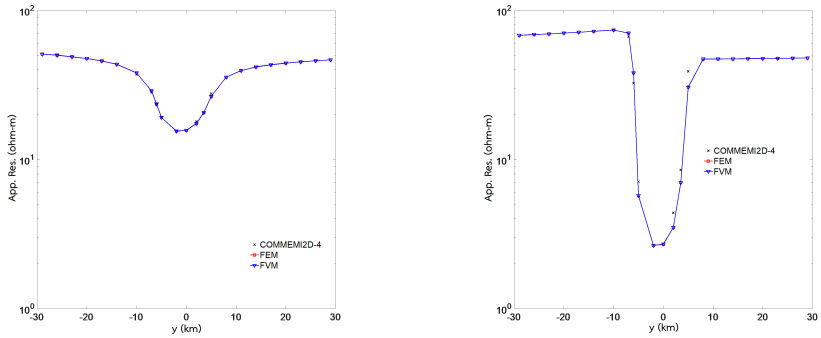

FIGURE 13. Apparent resistivity at period T = 100 seconds for TE-mode (left) and TM-mode (right).

method has more operations, our FV codes therefore take a longer time than FE codes about 40%.

6. Conclusions

This paper developed the FV method with unstructured quadrilateral mesh to solve 2-D MT problem. Our FV scheme provides a good accuracy of MT responses when it is tested on the half-space model. Furthermore, our FV codes give a better accuracy when compared to that of the FE method with the same mesh for all range of tested periods. It is indicated that the FV method do not use more density of volume to provide a good accuracy, but it requires only an appropriate local refinement mesh. For the reliability of codes, the obtained responses and those calculated by the COMMEMI projects [23] are comparable for two modes. These show that our FV codes are accurate and reliable. However, the efficiency our FV codes, which is considered in term of CPU time, is slower than that of the FE method with the same mesh because the processes to construct the coefficient matrix is more complicated. With these experiments, our FV codes may be an interesting numerical method to use as a forward solver for MT inversion algorithms in future.

Acknowledgements

This work has been supported by the Academic Affairs Promotion Fund, Faculty of Science, Khon Kaen University, Fiscal year 2561 (RAAPF), the National Research Council of Thailand and Khon Kaen University, Thailand (Grant Number 6200052) and the Smart Learning Innovation Research Center, Khon Kaen University, Thailand.

References

[1] T.D. Blacker, M.B. Stephenson, Paving. a new approach to automated quadrilateral mesh generation, International Journal for Numerical Methods in Engineering 32 (4) (1991) 811–847.

[2] M.N. Berdichevsky, V.I. Dmitriev, Models and methods of magnetotellurics, Springer, Berlin, 2008.

[3] M. Bern, Quadrilateral meshing by circle packing. International Journal of Computational Geometry & Applications (1997) 7–20.
[4] H.K. Du, Z.Y. Ren, J.T. Tang, A finite-volume approach for 2d magnetotellurics modeling with arbitrary topographies, Studia Geophysica et Geodaetica 60 (2) (2016) 332–347.
[5] A. Franke, R.U. Börner, K. Spitzer, Adaptive unstructured grid finite element simulation of two-dimensional magnetotelluric fields for arbitrary surface and seafloor topography, Geophysical Journal International 171 (1) (2007) 71–86.
[6] E. Haber, U.M. Ascher, Fast finite volume simulation of 3d electromagnetic problems with highly discontinuous coefficients, SIAM Journal of Scientific Computing 22 (6) (2001) 1943–1961.
[7] V. Hurtado, F. Sandro, C. Maliska, A. F. Carvalho da Silva, J. Cordazzo, A Quadrilateral Element-Based Finite-Volume Formulation for the Simulation of Complex Reservoirs, Paper presented at the Latin American & Caribbean Petroleum Engineering Conference, Buenos Aires, Argentina, 2007.
[8] J. Jin, The Finite Element Method in Electromagnetics. John Wiley & Sons, Inc., 2nd edition, 2002.
[9] K. Key, C. Weiss, Adaptive finite-element modeling using unstructured grids: The 2D magnetotelluric example, GEOPHYSICS 71 (6) (2006) G291–G299.
[10] S.K. Lee, H. Kim, Y. Song, C.K. Lee, MT2DInvMatlab-A program in MATLAB and FORTRAN for two-dimensional magnetotelluric inversion, Computers & Geosciences 35 (8) (2009) 1722–1734.
[11] D. Malleswari, K. Veeraswamy, Numerical simulation of coast effect on magnetotelluric measurements, Acta Geodaetica et Geophysica 49 (1) (2014) 17–35.
[12] S.J. Owen, A survey of unstructured mesh generation technology, International Meshing Roundtable (1998) 239–267.
[13] D. Pandey, M. Sinha, L. MacGregor, S. Singh, Ocean coast effect on magnetotelluric data: A case study from Kachchh, India. Marine Geophysical Researches 29 (3) (2008) 185–193.
[14] K.P. Rao, G.A. Babu, EMOD2D—a program in C++ for finite difference modelling of magnetotelluric TM mode responses over 2D earth. Computers & geosciences 32 (9) (2006) 1499–1511.
[15] I.K. Reddy, D. Rankin, Magnetotelluric response of laterally inhomogeneous and anisotropic media. GEOPHYSICS 40 (6) (1975) 1035–1045.
[16] J.F. Remacle, J. Lambrechts, B. Seny, E. Marchandise, A. Johnen, C.Geuzainet, Blossom-Quad: A non-uniform quadrilateral mesh generator using a minimum-cost perfect-matching algorithm. International Journal for Numerical Methods in Engineering 89 (9) (2012) 1102–1119.
[17] W. Sarakorn, 2-D magnetotelluric modeling using finite element method incorporating unstructured quadrilateral elements, J. Appl. Geophys. 139 (2017) 16–24.
[18] W. Sarakorn, C. Vachiratienchai, Hybrid finite difference-finite element method to incorporate topography and bathymetry for two-dimensional magnetotelluric modeling. Earth, Planets and Space 70 (1) (2018) 103.
[19] J. Sarrate, A. Huerta, Efficient unstructured quadrilateral mesh generation. International Journal for Numerical Methods in Engineering 49 (10) (2000) 1327–1350.
[20] T. Sonar, Classical Finite Volume Methods, North Holland, 2016.

[21] U.K. Singh, Y. Kant, R.P. Singh, Effect of coast on magnetotelluric measurements in India. Annals of Geophysics 38 (3-4) (1995).

[22] P.E. Wannamaker, J.A. Stodt, L. Rijo, Two-dimensional topographic responses in magnetotellurics modeled using finite elements, GEOPHYSICS 51 (11) (1986) 2131–2144.

[23] M.S. Zhdanov, I.M. Varentsov, J.T. Weaver, N.G. Golubev, V.A. Krylov, Methods for modelling electromagnetic fields results from COMMEMI - the international project on the comparison of modelling methods for electromagnetic induction. Journal of Applied Geophysics 37 (3-4) (1997) 133–271.